

# Ultralow radiative cooling of $C_n^-$ ( $n = 3-5$ )

Cite as: J. Chem. Phys. **151**, 114304 (2019); <https://doi.org/10.1063/1.5114678>

Submitted: 11 June 2019 . Accepted: 26 August 2019 . Published Online: 17 September 2019

James N. Bull , Michael S. Scholz , Eduardo Carrascosa , Moa K. Kristiansson , Gustav Eklund, Najeeb Punnakayathil, Nathalie de Ruelle, Henning Zettergren , Henning T. Schmidt , Henrik Cederquist, and Mark H. Stockett 



View Online



Export Citation



CrossMark

## ARTICLES YOU MAY BE INTERESTED IN

[Nonlinear transport coefficients from large deviation functions](#)

The Journal of Chemical Physics **151**, 014101 (2019); <https://doi.org/10.1063/1.5110507>

[Mobile obstacles accelerate and inhibit the bundle formation in two-patch colloidal particle](#)

The Journal of Chemical Physics **151**, 084901 (2019); <https://doi.org/10.1063/1.5110777>

[Microscopic derivation of coarse-grained, energy-conserving generalized Langevin dynamics](#)

The Journal of Chemical Physics **151**, 104109 (2019); <https://doi.org/10.1063/1.5096655>

## Lock-in Amplifiers up to 600 MHz

starting at

\$6,210



Zurich  
Instruments

Watch the Video 



# Ultralow radiative cooling of $C_n^-$ ( $n = 3-5$ )

Cite as: J. Chem. Phys. 151, 114304 (2019); doi: 10.1063/1.5114678

Submitted: 11 June 2019 • Accepted: 26 August 2019 •

Published Online: 17 September 2019



James N. Bull,<sup>1,a)</sup> Michael S. Scholz,<sup>2</sup> Eduardo Carrascosa,<sup>3</sup> Moa K. Kristiansson,<sup>4</sup> Gustav Eklund,<sup>4</sup> Najeeb Punnakayathil,<sup>4</sup> Nathalie de Ruelle,<sup>4</sup> Henning Zettergren,<sup>4</sup> Henning T. Schmidt,<sup>4</sup> Henrik Cederquist,<sup>4</sup> and Mark H. Stockett<sup>4,b)</sup>

## AFFILIATIONS

<sup>1</sup>School of Chemistry, Norwich Research Park, University of East Anglia, Norwich NR4 7TJ, United Kingdom

<sup>2</sup>School of Chemistry, University of Melbourne, Parkville, VIC 3010, Australia

<sup>3</sup>Laboratoire de Chimie Physique Moléculaire, École Polytechnique Fédérale de Lausanne, EPFL SB ISIC LCPM, Station 6, CH-1015 Lausanne, Switzerland

<sup>4</sup>Department of Physics, Stockholm University, SE-10691 Stockholm, Sweden

<sup>a)</sup>Electronic mail: james.bull@uea.ac.uk

<sup>b)</sup>Electronic mail: mark.stockett@fysik.su.se

## ABSTRACT

Ultralow radiative cooling lifetimes and adiabatic detachment energies for three astrochemically relevant anions,  $C_n^-$  ( $n = 3-5$ ), are measured using the Double ElectroStatic Ion Ring ExpERiment (DESIREE) infrastructure at Stockholm University. DESIREE maintains a background pressure of  $\approx 10^{-14}$  mbar and temperature of  $\approx 13$  K, allowing storage of mass-selected ions for hours and providing conditions coined a “molecular cloud in a box.” Here, we construct two-dimensional (2D) photodetachment spectra for the target anions by recording photodetachment signal as a function of irradiation wavelength and ion storage time (seconds to minute time scale). Ion cooling lifetimes, which are associated with infrared radiative emission, are extracted from the 2D photodetachment spectrum for each ion by tracking the disappearance of vibrational hot-band signal with ion storage time, giving  $\frac{1}{e}$  cooling lifetimes of  $3.1 \pm 0.1$  s ( $C_3^-$ ),  $6.8 \pm 0.5$  s ( $C_4^-$ ), and  $24 \pm 5$  s ( $C_5^-$ ). Fits of the photodetachment spectra for cold ions, i.e., those stored for at least 30 s, provide adiabatic detachment energies in good agreement with values from laser photoelectron spectroscopy on jet-cooled anions, confirming that radiative cooling has occurred in DESIREE. Ion cooling lifetimes are simulated using a simple harmonic cascade model, finding good agreement with experiment and providing a mode-by-mode understanding of the radiative cooling properties. The 2D photodetachment strategy and radiative cooling modeling developed in this study could be applied to investigate the ultraslow cooling dynamics of a wide range of molecular anions.

Published under license by AIP Publishing. <https://doi.org/10.1063/1.5114678>

## I. INTRODUCTION

Which molecular anions exist in space? What are their formation mechanisms and life cycles? These are two long-standing questions in astrochemistry.<sup>1,2</sup> Prior to a decade and a half ago,  $H^-$  was the only anion thought to play a prominent role in the interstellar medium (ISM). In 2006, the first molecular anion,  $C_6H^-$ , was discovered by comparing astronomical line spectra with gas-phase action spectra recorded in the laboratory.<sup>3</sup> Over the next four years, there were five further identifications:  $C_4H^-$ ,<sup>4</sup>  $C_8H^-$ ,<sup>5</sup>  $CN^-$ ,<sup>6</sup>  $C_3N^-$ ,<sup>7</sup> and  $C_5N^-$ .<sup>8</sup> Vibrationally excited  $C_6H^-$  was also detected alongside  $C_5N^-$ .<sup>8</sup> However, despite increasing interest in the role of

molecular anions in space, there has been a stall in new identifications. It is thought that the discovery of new molecular anions is thwarted by a lack of understanding of the formation mechanism(s) and dynamical properties of both the anions known to exist in the ISM and new anions yet to be assigned.<sup>2,9</sup> Dynamical properties in this context include electron capture cross sections, electronic internal conversion efficiencies, couplings between dipole-bound and valence-localized states, cross sections for neutralization reactions with cations, and the rates of radiative cooling.<sup>10,11</sup> As an example of the need for reliable measurements of the dynamical properties of astrochemically relevant anions, in a discussion on radiative electron attachment (which involves formation of a

vibrationally excited ground state ion that must cool) Herbst<sup>12</sup> remarked “*The discovery of molecular anions [in space] has generated the need to include their formation and destruction in chemical models . . . the larger [carbonaceous] molecular anions detected ( $n = 6, 8$ ) have higher abundances relative to their neutral precursors because the radiative attachment rate increases with the number of degrees of freedom of the anion. However, their rate estimates are quite uncertain and experimental studies are highly welcome.*” Although gas-phase action spectroscopies can provide data on electronic transitions and detachment energies for carbonaceous anions,<sup>13</sup> some of their dynamical properties such as infrared (IR) radiative cooling lifetimes are more difficult to measure because hot anions need to be isolated (i.e., free from collision) for periods of milliseconds to minutes. These conditions are not attainable with conventional ion traps.

Here, we used the Double ElectroStatic Ion Ring ExpERiment (DESIREE) infrastructure at Stockholm University to characterize the radiative cooling lifetimes and adiabatic detachment energies (ADEs) of  $C_n^-$  ( $n = 3-5$ ) by monitoring the intensity of vibrational hot bands near the electron detachment threshold with ion storage time. The present investigation targeted the  $C_n^-$  ( $n = 3-5$ ) species because they are likely ISM anions. In particular, they possess similar bonding and electronic structure to the molecular anions already known to exist in the ISM, they could be formed through either photodissociation or dissociative electron attachment mechanisms,<sup>1,2</sup> and neutral  $C_3$  and  $C_5$  are known interstellar molecules.<sup>14,15</sup> Although anions are unlikely to be significant astrochemical species in “photon-dominated regions” (PDRs, e.g., diffuse clouds) due to facile destruction by photodetachment with visible and ultraviolet light,<sup>2,16</sup> the abundance of anions in dark clouds (e.g.,  $C_6H^-$  in L1527)<sup>17</sup> has been shown to reach nearly 10% of that for the corresponding neutral molecule, suggesting that the negative charge in photon-free regions of space is more likely in the form of anions than free electrons. Cold dark molecular clouds have temperatures of 10–20 K,<sup>18</sup> the normal operating temperature of DESIREE ( $\approx 13$  K) is squarely within this range.<sup>19</sup>

In the absence of collisional quenching, the spontaneous cooling dynamics of hot molecular anions such as  $C_n^-$  ( $n = 3-5$ ) can be divided into three time ( $t$ ) regimes:

- Statistical regime I ( $t \leq 10^{-3}$  s): Internal energy is high, e.g., several electron-volts above the thresholds for dissociation, thermionic emission,<sup>20</sup> and recurrent/Poincaré fluorescence.<sup>21</sup> The energy threshold for thermionic emission is the ADE, which for  $C_n^-$  ( $n = 3-5$ ) is  $\approx 2-4$  eV, and the energy threshold for dissociation can be approximated by the lowest bond dissociation energy ( $\approx 3-4$  eV). Both thermionic emission and dissociation result in destruction of the anion. Recurrent fluorescence, which is known for  $C_4^-$  and  $C_6^-$ ,<sup>22-25</sup> involves inverse internal conversion to an electronic excited state (situated below the ADE, e.g.,  $\approx 2-3$  eV) followed by radiative emission.<sup>26</sup>
- Slow regime II ( $t \approx 10^{-3}-1$  s): Internal energy is in the vicinity of the lowest thresholds for the cooling mechanisms important for regime I, e.g.,  $\sim 2$  eV. In addition to slow cooling through these mechanisms, radiative emission due to vibrational transitions becomes important.

- Ultraslow regime III ( $t \gtrsim 1$  s): Internal energy is below the thresholds for dissociation, thermionic emission, and recurrent fluorescence. Ions cool only through radiative vibrational (IR) transitions and rotational (microwave) transitions, with vibrational cooling occurring much faster than rotational cooling.<sup>19,27</sup> Cooling dynamics in this regime have been explored for only a few small anions due to technical challenges associated with isolating ions for duration extending to minutes and maintaining low background temperatures.<sup>28-33</sup>

While the target anions in this work have been intensively studied by several groups in recent years, all of these earlier works used room-temperature electrostatic ion storage rings or beam traps and were limited to characterizing cooling dynamics occurring on subsecond time scales.<sup>23,25,34-37</sup> In the present study, we have used the DESIREE infrastructure to investigate the cooling dynamics of the target anions on the ultraslow,  $t \gtrsim 1$  s time scale. Our strategy involved storing ions for up to  $\approx 1$  min and monitoring the intensity of hot bands with ion storage time, providing an indirect characterization of cooling lifetimes. The  $\frac{1}{6}$  ion cooling lifetimes, which are attributed to IR radiative emission, are well-described by a simple harmonic cascade model of this process. Fits of the cold photodetachment spectra associated with ions stored for at least 30 s to the Wigner threshold law demonstrate an alternative, cryogenic method for obtaining ADE values. The ADEs provide a useful reference for comparison of 2D data with conventional jet-cooled measurements for demonstrating cooling (depletion) of hot bands.

## II. METHODS

DESIREE is a cryogenic dual electrostatic ion storage ring facility located at the Department of Physics, Stockholm University.<sup>38,39</sup> The major components constituting the so-called “symmetric” storage ring are schematically illustrated in Fig. 1. The interior of the ring is cooled to  $\approx 13$  K by compressed helium refrigerators and is isolated from external thermal radiation by several layers of insulation.<sup>19</sup> Vacuum is maintained at a background pressure of  $\approx 10^{-14}$  mbar using cryopumping combined with turbomolecular pumps and oil-free backing pumps. These ultrahigh vacuum conditions allow storage of kiloelectronvolt ion beams for hours.<sup>40</sup> In the present experiments, the target anions [ $C_n^-$  ( $n = 3-5$ )] were produced using a cesium sputtering ion source with a graphite cathode.<sup>39</sup> This process generates ions with a high degree of rovibrational excitation, i.e., source-heated ions. The nascent ions were accelerated to 10 keV, selected according to their mass-to-charge ratio using a bending magnet, and injected into the symmetric ion storage ring. Transport from the source to the ring takes  $\approx 100$   $\mu$ s. The  $\frac{1}{6}$  beam storage lifetimes were measured at  $540 \pm 30$  s for  $C_3^-$  and  $570 \pm 30$  s for  $C_5^-$  (see the [supplementary material](#)). Although the beam storage lifetime for  $C_4^-$  was not measured in this study, we expect a similar lifetime to those for  $C_3^-$  and  $C_5^-$ . These beam storage lifetimes are limited by loss of ions through collisions with background gas.<sup>39</sup>

### A. One-color experiments

In the one-color experiments, stored ions were irradiated with tunable-wavelength light from an optical parametric oscillator

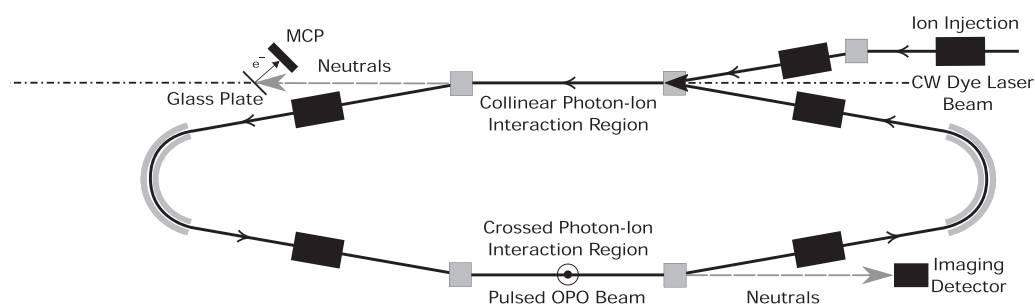


**FIG. 1.** The symmetric ion storage ring in DESIREE.<sup>38,39</sup> Neutral particles formed by photodetachment in the lower straight region (crossed-beam geometry with the optical parametric oscillator, OPO) are detected in their forward directions with the “imaging detector.” In another set of measurements on  $C_3^-$ , light from a cw dye laser was merged collinearly with the stored ion beam in the upper straight section. The wavelength of the cw light was tuned to be in resonance with the vibrational hot band of  $C_3^-$  (620.5 nm). The ring circumference is 8.6 m and each straight section has a length of 0.96 m.

(OPO, EKSPLA NT342B, 10 Hz) using a crossed-beam arrangement through one of the straight sections of the ion storage ring (see Fig. 1). Any neutral particles formed through photodetachment or photodissociation are unaffected by the ring’s electrostatic steering fields and impact on a microchannel plate (MCP) detector (“imaging detector” in Fig. 1).<sup>41</sup> The signal from the MCP detector was gated using a 1  $\mu$ s duration pulse that was slightly delayed with respect to the OPO pulse to account for the neutral particle’s flight time from the interaction region to the detector. The purpose of the gate was to eliminate the signal from scattered OPO light striking the detector and to minimize background counts from collision-induced detachment events due to the residual gas consisting of  $\sim 10^4$   $H_2$  molecules per  $cm^3$ . The OPO wavelengths were calibrated using an optical spectrograph (Avantes AvaSpec-3648), which was itself calibrated against a wavemeter (HighFinesse WS-8) using a diode laser (632.6 nm). The irradiation wavelength was stepped in 0.5 nm increments (2 nm for  $C_4^-$ ) between ion injections for a given ion storage time, providing a two-dimensional (2D) photodetachment spectrum, i.e., a series of photodetachment spectra as a function of wavelength and ion storage time (see Refs. 19 and 27 for a similar procedure applied to rotational cooling of  $OH^-$ ). For a given ion, the time evolution of the photodetachment yield at a specific wavelength or range of wavelengths can be obtained by taking a wavelength slice through the 2D photodetachment spectrum.

Part of our interpretation applied Principal Component Analysis (PCA)<sup>42</sup> to the 2D photodetachment spectrum for each ion. PCA is a statistical procedure that decomposes a multidimensional dataset  $X$  into a set of orthogonal principal components (PCs) which are the eigenvectors of the covariance matrix  $X^T X$ . Here,  $X$  is the  $m \times n$  matrix of photodetachment spectra, each measured at  $m$  OPO wavelengths, recorded at  $n$  different storage times. The eigenvalues associated with each PC relate to the fraction of the variation in  $X$  that is explained by each PC, and the principal values (PVs, the projection of  $X$  on its PCs) give the weight of each PC as a function of time. In the present case, the  $n$  PCs may be thought of as the basis set of elementary spectra that describe the evolution (due to radiative cooling of the ions) of the photodetachment spectrum with ion storage time, with a time invariant background due to the

photodetachment signal from cold ions (or nearly time invariant because of a finite ion beam storage lifetime).<sup>43</sup> PCA can be used to extract the cold-ion photodetachment spectrum and radiative cooling rates using the full 2D action spectrum, rather than arbitrary time and wavelength slices, improving signal-to-noise and eliminating innate human bias. The cooling lifetimes obtained from the PVs should be considered wavelength-averaged values since each probe wavelength provides a slightly different ion cooling lifetime due to a distribution of internal vibrational energies in the stored ion beam.

## B. Deplete-probe experiments on $C_3^-$

Deplete-probe experiments on source-heated  $C_3^-$  were performed by adapting the procedure recently described by Schmidt *et al.*,<sup>19</sup> where the effect of the depletion laser was to preferentially photodetach rotationally excited ions and thus reduce the measured ion cooling lifetimes. Depletion involved intercepting the stored ion beam with 620.5 nm light from a cw laser (Coherent 899 ring dye laser) using a merged-beam geometry in the straight section of the ion storage ring opposite the OPO light interaction region (see Fig. 1). The depletion laser wavelength (620.5 nm or 1.998 eV) was chosen to be close to the ADE from the present measurements (see below) because the photodetachment cross section for vibrationally excited (hot band)  $C_3^-$  is much larger than that for cold ions.

## C. Adiabatic detachment energies

The adiabatic detachment energy (ADE) for the target anions were extracted from the cold photodetachment spectrum assuming fit with the Wigner threshold law,<sup>44,45</sup>

$$\sigma_{PD} = (E_{kin})^{L+\frac{1}{2}}, \quad (1)$$

where  $\sigma_{PD}$  is the photodetachment cross section,  $E_{kin}$  is the kinetic energy of the ejected electron (energy in excess of the ADE for a direct photodetachment process), and  $L$  is the angular momentum of the outgoing electron. For the present systems which involve photodetachment from the  $\pi$  molecular orbital, we find that  $L = 2$  ( $d$  wave photoelectron) provided best fit to the experimental data.

The ADE is taken to be the energy at which the Wigner threshold law fit exceeds  $3\sigma$  of the baseline signal (nonzero baseline due to dark counts). We note that the above expression is strictly valid for atomic species; the best fit values of  $L$  can deviate from integers for molecules—although in the present case freeing  $L$  did not improve the quality of the fit—see example fits in the [supplementary material](#). The error bars reported for the ADE determinations are the statistical uncertainties from the fits to the threshold law (contributions from laser wavelength calibration and bandwidth are small).

#### D. Radiative cooling lifetime modeling

Spontaneous cooling in the present experiments is presumed to occur through IR radiative emission. A simple harmonic cascade (SHC) model of this process was developed to interpret the experimental results. The model assumes vibrational density of states  $\rho$  computed using the Beyer-Swinehart algorithm using anharmonic or scaled harmonic vibrational mode frequencies  $\nu_s$  calculated at the  $\omega$ B97X-D//aug-cc-pVTZ level of theory with computational package Q-Chem 4.4 (see the [supplementary material](#)).<sup>46–48</sup> For a given mode  $s$ , the IR radiative cooling rate coefficient, assuming only transitions where  $\Delta v_s = -1$  are allowed, with  $v$  being the vibrational quantum number, is<sup>36</sup>

$$k_s(E) = A_s^{10} \sum_{v=1}^{v \leq E/h\nu_s} \frac{\rho(E - hv_s)}{\rho(E)}, \quad (2)$$

where  $E$  is the energy of a given vibrational state,  $h$  is Planck's constant, and the summation is over  $v$  ( $v = 0$  and  $1$  are the ground and first excited vibrational states of mode  $s$ , respectively). The Einstein coefficients  $A_s^{10}$  were calculated at the  $\omega$ B97X-D//aug-cc-pVTZ within the harmonic approximation (see the [supplementary material](#)) and are assumed to be independent of  $v$ . Starting from an initial Boltzmann distribution of vibrational energy  $g(E, t = 0)$  corresponding to 1000 K, the population in each level was recalculated at each simulation time step. The model allowed for two treatments of intramolecular vibrational energy redistribution (IVR),<sup>49</sup> i.e., statistical randomization of vibrational energy with time,  $t$ :

- (i) IVR is negligible or slow compared with radiative cooling—the population of each mode is explicitly tracked according to the following expression:

$$g(E, t + dt) = \sum_s g(E, t) e^{-k_s(E)dt} + \sum_s g(E + h\nu_s, t) (1 - e^{-k_s(E+h\nu_s)dt}). \quad (3)$$

- (ii) IVR is fast compared with radiative cooling—vibrational energy is statistically redistributed each simulation time step and the total energy emitted radiatively at each time step is

$$dE_{tot}/dt = - \int g(E, t) \sum_s h\nu_s k_s(E) dE, \quad (4)$$

where the total energy remaining in the ensemble as a function of time  $E_{tot}(t) = \int E g(E, t) dE$  was taken as an indicator of the progress of cooling. Given that the vibrational energy quanta are small and

the number of stored ions is large, level occupation numbers were treated as continuous quantities. We expect that case (ii) should be most relevant for the present source-heated anions because ion cooling lifetimes are long (seconds time scale) compared with the expected time scale for IVR (nanoseconds to millisecond time scale).

The SHC modeling starts from a hot ensemble and simulates the internal energy as a function of ion storage time. For case (i), the internal vibrational energy reached a nonzero asymptotic value because any population that was portioned to IR inactive modes is not emitted radiatively. For case (ii), because the lowest frequency vibrational modes for each anion are IR active, all vibrational energy in excess of the zero-point energy can be liberated and thus the model goes asymptotically to zero vibrational energy at long times. To facilitate visual comparison of case (ii) with case (i) and with experiment, a constant offset has been added to case (ii) results that are equal to the asymptotic value of a fit of the experimental data to a (multi)exponential function. Furthermore, it was found that the initial temperature assumed in the SHC model (e.g., 500–5000 K) altered the cooling dynamics only on time scales much faster than those probed in the present experiments, e.g., milliseconds.

It is worth noting that use of the commonly cited harmonic frequencies and intensities from Szczepanski *et al.*<sup>50</sup> calculated at the B3LYP//6-31G\* level of theory within the SHC framework produced qualitatively similar results to those presented in this study, but required scaling the  $A_s^{10}$  coefficients with factor 0.5 for best agreement between modeled ion cooling lifetimes and experimental values.

### III. RESULTS AND DISCUSSION

#### A. Tricarbon anion, $C_3^-$

The 2D photodetachment spectrum for  $C_3^-$  as a function of ion storage time is shown in the upper panel of [Fig. 2](#). An alternative representation of the data is shown in the middle panel of [Fig. 2](#), where the spectra have been divided into four time bins, with the 0–3 s time bin corresponding to ions recently injected into the storage ring and the 30–57 s time bin corresponding to ions that have been stored for at least 30 s. The time-binned photodetachment spectra show a broad feature over the expected ADE ( $1.99 \pm 0.025$  eV or  $622 \pm 8$  nm from photoelectron spectroscopy)<sup>51</sup> due to vibrationally excited  $C_3^-$  ions that cool over the first <30 s, providing a “cold” photodetachment spectrum (30–57 s spectrum). A fit of the cold photodetachment spectrum with the Wigner threshold law gave ADE =  $1.990 \pm 0.005$  eV ( $623 \pm 0.6$  nm), which is within the error of the earlier photoelectron spectroscopy determination.

The lower panel of [Fig. 2](#) shows the photodetachment signal with ion storage time (1 s time bins) at six selected wavelengths, i.e., horizontal cuts in the upper panel of [Fig. 2](#). Fits with a single-exponential decay curve gave lifetimes ranging from  $4.3 \pm 0.8$  s (590 nm) to  $1.8 \pm 0.2$  s (615 nm), demonstrating that cooling occurs more slowly for anions probed at a shorter wavelength, i.e., those closer to the detachment threshold (the error bars here and for all lifetime determinations are the statistical uncertainties from the fitting procedure). This is readily interpreted in terms of [Eq. \(2\)](#), which indicates that the cooling rate rapidly increases with vibrational excitation and that the variation in ion cooling lifetime is due to the stored ion beam having a distribution of internal vibrational energies.

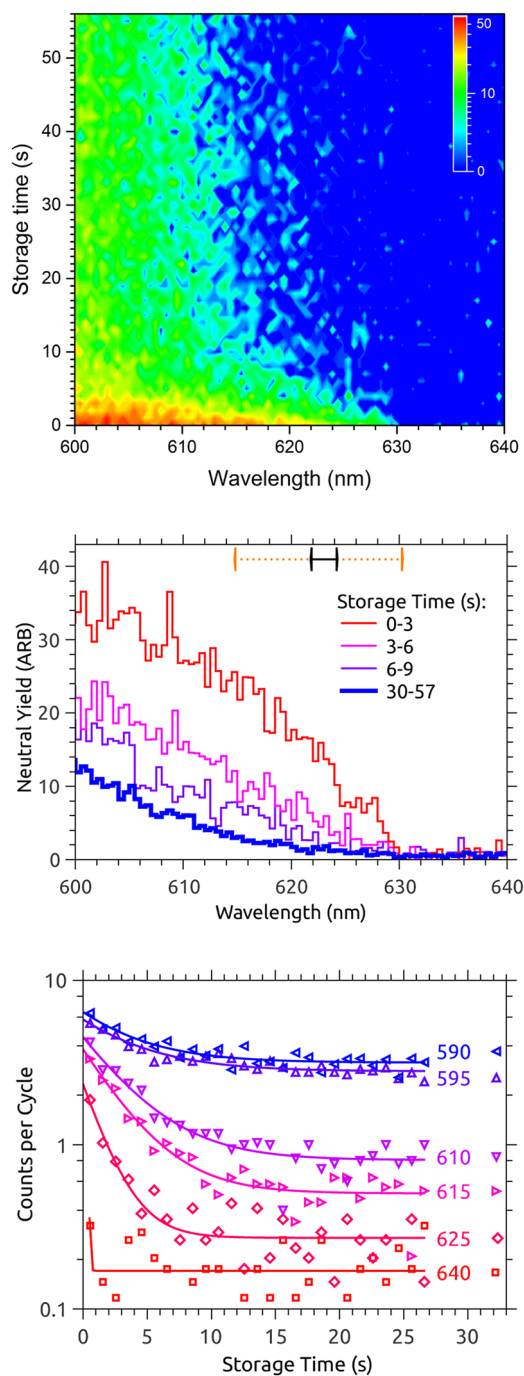


**FIG. 2.** Upper panel: 2D photodetachment spectrum (neutral yield vs wavelength and storage time) for  $C_3^-$ . Note the logarithmic color scale. Middle panel: Time-binned photodetachment spectra for  $C_3^-$ . The black bar represents the ADE and uncertainty determined for ions stored at least 30 s, and the orange bar corresponds to the photoelectron spectroscopy value from Ref. 51. Lower panel: Decay of the photodetachment signal with ion storage time at selected probe wavelengths (note the log scale). Time constants for single-exponential fits in the lower panel are  $4.3 \pm 0.8$  s (590 nm),  $4.6 \pm 0.7$  s (595 nm),  $3.8 \pm 0.4$  s (610 nm),  $3.2 \pm 0.2$  s (615 nm), and  $1.8 \pm 0.2$  s (625 nm).

Principal component analysis (PCA) of the 2D photodetachment spectrum for  $C_3^-$  suggested a single principal component (PC1 in Fig. 3) describes the hot-band intensity with ion storage time. Nearly 80% of the variance in the 2D spectrum is explained by PC1, with the remaining PCs describing only statistical fluctuations with no secular time dependence. The principal values of PC1 (denoted PV1) with ion storage time are shown in the lower panel of Fig. 3. The fit of PV1 with a biexponential gave a fast lifetime of  $3.1 \pm 0.1$  s, which, as expected, is intermediate between the lifetimes for the wavelength-selected cooling times in the lower panel of Fig. 2. The second lifetime ( $>200$  s) is much longer than the measurement cycle (60 s for  $C_3^-$ ) and is presumably associated with the beam storage lifetime ( $540 \pm 30$  s for  $C_3^-$ , see the [supplementary material](#)). The time-invariant cold spectrum (Fig. 3, upper panel) was obtained by subtracting PC1, weighted by PV1, from the 2D photodetachment spectrum. This closely resembles the cold spectrum in the middle panel of Fig. 2, but utilizes the entire dataset rather than arbitrarily time-binned data. The fit of the cold spectrum from PCA with the Wigner threshold law gave an ADE of  $1.987 \pm 0.004$  eV

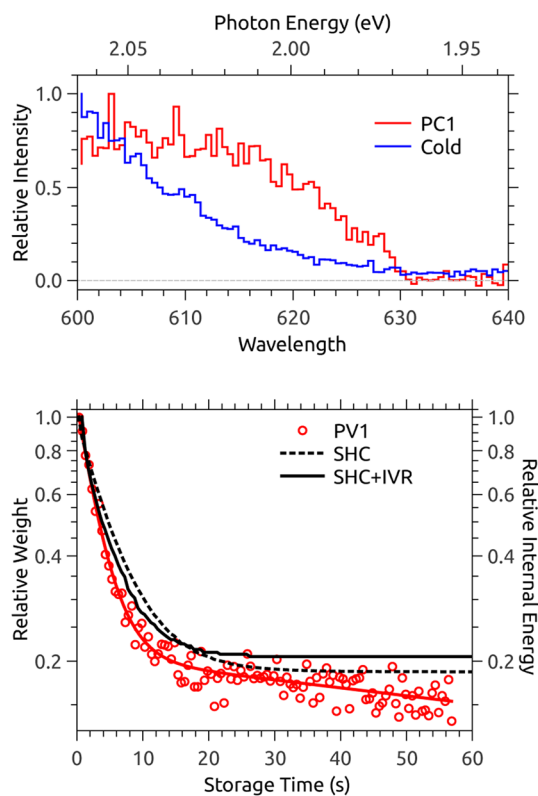


**FIG. 3.** Principal component analysis on  $C_3^-$ . Upper panel: Principal component (PC1) and cold photodetachment spectrum normalized so that the maximum of each curve is unity. Lower panel: Principal values for PC1 (denoted PV1, left axis) with ion storage time and total internal energy ( $E_{tot}$ ) from the SHC radiative cooling model (right axis, same scale). Each curve is normalized so that the value at the first time point is unity (note the log scale). The gradual decrease in PV1 for ion storage times longer than  $\approx 20$  s is attributed to the beam storage lifetime in DESIREE.

(624.0 ± 0.6 nm), which is within the error of the above determination using the cold, time-binned photodetachment spectrum.

IR radiative cooling characteristics for  $C_3^-$  from the SHC model are summarized in the lower panel of Fig. 3. The dashed black curve assumes the case of no IVR and the solid black curve includes IVR. Exponential fits to the SHC curves returned ion cooling lifetimes of  $5.22 \pm 0.01$  s (no IVR) and  $3.68 \pm 0.06$  s (including IVR). The latter is in reasonable agreement with the average ion cooling lifetime from PCA ( $3.1 \pm 0.1$  s).

The influence of the cw laser (620.5 nm) on the cooling lifetimes of  $C_3^-$  is shown in Fig. 4. Comparison of cw laser ON (black) with cw laser OFF (red) data at the probe wavelengths of 615, 610, 595, and 590 nm show a systematic decrease in the ion cooling lifetimes by  $\approx 1$  s because the photodetachment cross section is larger for vibrationally excited ions than for cold ions at 620.5 nm. No such effect was observed at 625 nm, i.e., probe wavelength longer than that of the cw laser. These data provide a proof-of-principle measurement demonstrating a deplete-probe scheme to preferentially remove hot ions from the stored ion beam. The extent of depletion could likely be improved through better overlap of the cw beam with the ion beam and increase in the cw laser power.

## B. Tetracarbon anion, $C_4^-$

Time-binned photodetachment spectra and PCA on the 2D photodetachment spectrum for  $C_4^-$  are summarized in the upper and middle/lower panels of Fig. 5, respectively. The  $C_4^-$  photodetachment data were recorded in larger wavelength increments compared with  $C_3^-$  or  $C_5^-$  due to substantially lower laser fluence from the OPO at the near-UV wavelengths needed for photodetachment. The time-binned photodetachment spectra for  $C_4^-$  indicate that the hot-band signal has disappeared after  $\approx 30$  s. The fit of the 30–55 s time-binned spectrum with the Wigner threshold law gave an ADE of  $3.83 \pm 0.03$  eV (323.7 ± 2.5 nm), which is consistent with the value from photoelectron spectroscopy ( $3.882 \pm 0.010$  eV).<sup>51</sup>

Application of PCA to the 2D photodetachment spectrum of  $C_4^-$  again suggested that a single principal component (PC1 in Fig. 5, middle panel) describes the variation in the hot band intensity with ion storage time. The principal value of PC1 with ion storage time

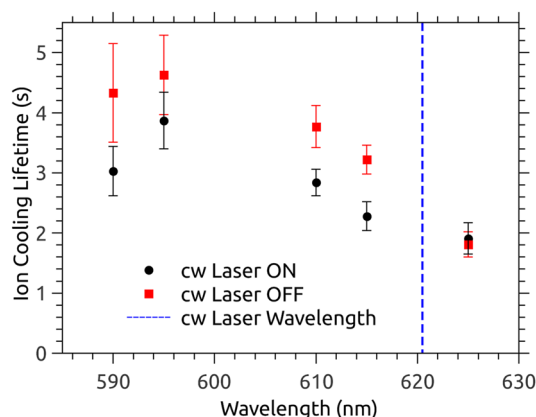


**FIG. 4.** Cooling lifetimes for  $C_3^-$  using the deplete-probe scheme. The black circles and red squares are cooling lifetimes with and without irradiation using cw laser light at 620.5 nm (dashed blue vertical line).

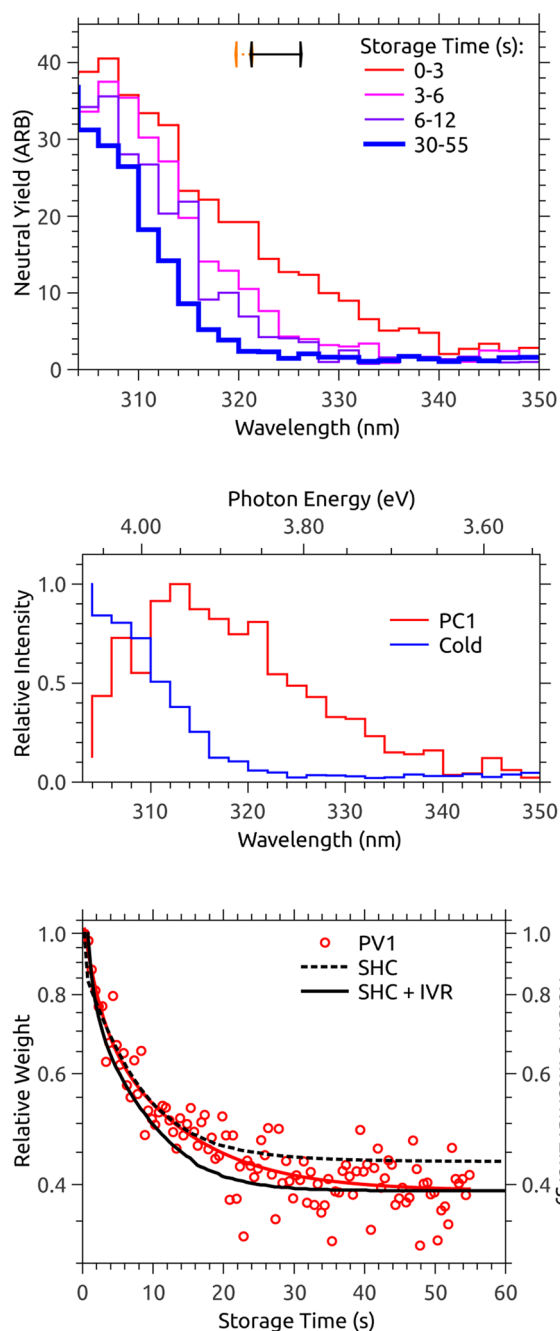


**FIG. 5.** Upper panel: Time-binned photodetachment spectra for  $C_4^-$ , recorded by monitoring the yield of neutral particles with the wavelength of light. The black bar represents the ADE and uncertainty determined for ions stored at least 30 s, and the orange bar corresponds to the photoelectron spectroscopy value from Ref. 51. Middle panel: Principal component (PC1) and cold photodetachment spectrum from the 2D photodetachment spectrum of  $C_4^-$  normalized so that the maximum of each curve is unity. Lower panel: Principal values for PC1 (denoted PV1, left axis) with ion storage time and total internal energy ( $E_{tot}$ ) from the SHC radiative cooling model (right axis, same scale). Each curve is normalized so that the value at the first time point is unity (note the log scale).

(PV1 in Fig. 5, lower) has a fitted lifetime of  $6.8 \pm 0.5$  s, which is roughly twice that for  $C_3^-$  and comparable with the wavelength-binned values given above. Unfortunately, the data are of insufficient quality for a biexponential fit to account for the beam storage lifetime. As for  $C_3^-$ , shorter wavelengths are associated with longer ion cooling lifetimes—see the [supplementary material](#) for further details. The fitted ADE for the PCA-derived cold ion spectrum is  $3.82 \pm 0.03$  eV, which is in good agreement with the cold, time-binned photodetachment spectrum value ( $3.83 \pm 0.03$  eV).

IR radiative cooling lifetimes for  $C_4^-$  from the SHC model are  $6.74 \pm 0.01$  s (no IVR) and  $5.4 \pm 0.1$  s (including IVR), which are both in reasonable agreement with the lifetime from PCA of  $6.8 \pm 0.5$  s.

### C. Pentacarbon anion, $C_5^-$

The 2D photodetachment spectrum, time-binned photodetachment spectra, and PCA for  $C_5^-$  are summarized in Figs. 6 and 7,

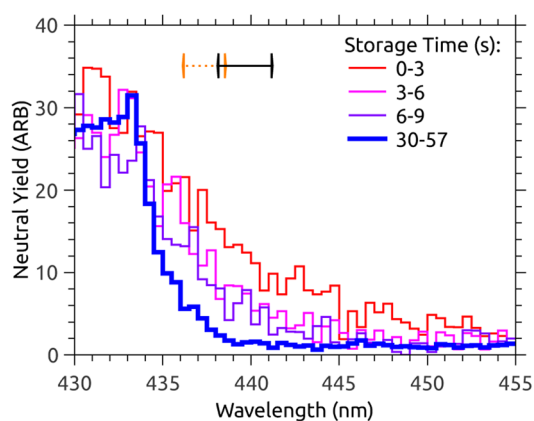
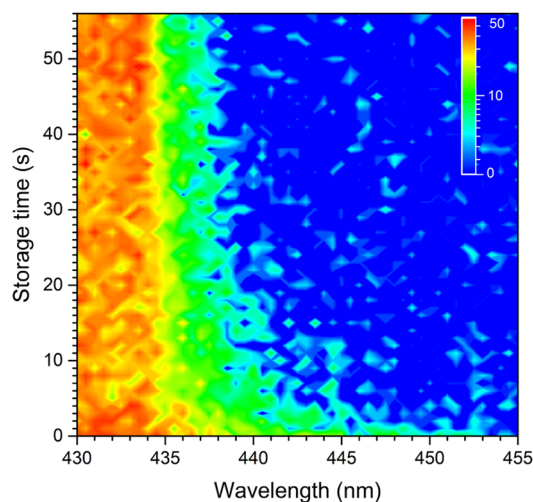


**FIG. 6.** Upper panel: 2D photodetachment spectrum (neutral yield vs wavelength and storage time) for  $C_5^-$ . Note the logarithmic color scale. Lower panel: Time-binned photodetachment spectra for  $C_5^-$ . The black bar represents the ADE and uncertainty determined for ions stored at least 30 s, and the orange bar corresponds to the photoelectron spectroscopy value from Ref. 51.

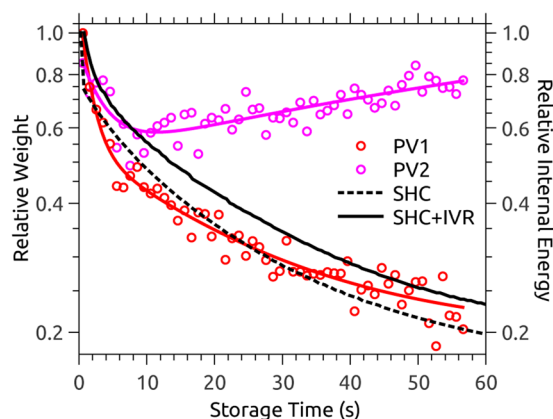
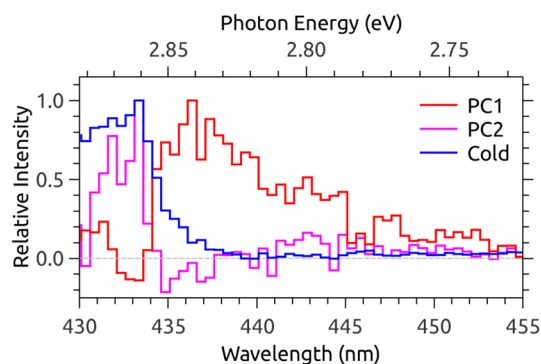


**FIG. 7.** Upper panel: Principal components (PC1 and PC2) and cold photodetachment spectrum extracted from the 2D photodetachment spectrum of  $C_5^-$  normalized so that the maximum of each curve is unity. Lower panel: Principal values for PC1 and PC2 (denoted PV1 and PV2, left axis) with ion storage time and total internal energy ( $E_{tot}$ ) from the SHC radiative cooling model (right axis, same scale). Each curve is normalized so that the value at the first time point is unity (note the log scale).

respectively. In comparison to  $C_3^-$  (Fig. 2, upper panel), it is clear from the 2D spectrum of  $C_5^-$  (Fig. 6, upper panel) that a larger fraction of the yield at short wavelengths (photon energies above the ADE) remains at long storage times. Intriguingly, the cooling behavior presents a different situation compared with  $C_3^-$  and  $C_4^-$ . Whereas the hot band photodetachment signal at wavelengths longer than  $\approx 435$  nm diminishes over the first few seconds of ion storage, there is an enhancement of the photodetachment signal for wavelengths shorter than  $\approx 435$  nm (i.e., above the ADE, most clearly visible comparing the 6–9 s and 30–57 s time-binned spectra in Fig. 6, lower panel), which will be discussed soon. The fit of the 30–57 s “cold” time-binned spectrum (Fig. 6, lower panel) with the Wigner threshold law gave ADE =  $2.82 \pm 0.01$  eV ( $439.7 \pm 1.6$  nm), which agrees with the value from photoelectron spectroscopy ( $2.839 \pm 0.008$  eV).<sup>51</sup>

Ion cooling lifetimes at selected probe wavelengths are  $22 \pm 3$  s (435 nm),  $7.7 \pm 0.8$  s (440 nm), and  $5.7 \pm 0.6$  s (445 nm)—see the [supplementary material](#) for further details. As for  $C_3^-$  and  $C_4^-$ , shorter wavelengths are associated with longer ion cooling lifetimes.

Application of PCA to the 2D photodetachment spectrum of  $C_5^-$  suggested that two principal components (PC1 and PC2 in Fig. 7, upper panel) are necessary to describe the spectral variation with ion storage time. PC1 has a similar wavelength dependence and principal value (PV1) with ion storage time when compared with PC1 for  $C_3^-$  or  $C_4^-$ . PV1 was best fit with two exponential lifetimes of  $1.7 \pm 0.3$  s and  $24 \pm 5$  s, although there is also an unresolved long-lifetime decay associated with the beam storage lifetime. PC2 (Fig. 7, upper panel) resembles a vibrational peak for wavelengths just shorter than the ADE wavelength. The fit of the principal values for PC2 with ion storage time (PV2 in Fig. 7, lower panel) required both exponential decay and growth functions. The growth lifetime for PC2 is within the error of the long decay lifetime associated with PC1 (i.e., after  $\approx 10$  s, PV1 + PV2 is roughly steady state), implying that the hot band population associated with PC1 eventually contributes to PC2 at a longer ion storage time. We predominately assign PC2 to the  ${}^1\Sigma_g^+(v' = 0) \leftarrow {}^2\Pi_{3/2}(v'' = 0)$  detaching transition, which occurs at a slightly longer wavelength ( $\approx 0.5$  nm) than the alternative  ${}^1\Sigma_g^+(v' = 0) \leftarrow {}^2\Pi_{1/2}(v'' = 0)$  spin-orbit detaching transition.<sup>51–53</sup> Assuming this assignment is correct, it appears that as ions cool, the relative population of ground vibrational state anions

increases and the apparent photodetachment cross section for resonant photodetaching transitions increases. Consequently, the long lifetime associated with PC2 is due to decay of population associated with the  ${}^1\Sigma_g^+(v'_{1,2} = 1) \leftarrow {}^2\Pi_{3/2}(v''_{1,2} = 1)$  and  ${}^1\Sigma_g^+(v'_{1,2} = 1) \leftarrow {}^2\Pi_{1/2}(v''_{1,2} = 1)$  hot band detaching transitions (note that  $v_{1,2}$  in the present labeling scheme is equivalent to  $v_{6,7}$  in the Herzberg scheme in Refs. 51–53). The fitted ADE for the PCA-derived cold spectrum is  $2.82 \pm 0.03$  eV, which is that from the 30–57 s time-binned photodetachment spectrum.

The IR radiative cooling characteristics for  $C_5^-$  from the SHC model are summarized in Fig. 7, lower panel. Neglect of IVR in the modeling resulted in a cooling curve that was best fit with two lifetimes of  $4.78 \pm 0.08$  s and  $21.7 \pm 0.1$  s. Inclusion of IVR gave fitted lifetimes of  $1.63 \pm 0.04$  s and  $22.0 \pm 0.2$  s, which are in good agreement with values from PCA.

The need for a biexponential fit for  $C_5^-$  can be traced to mode-specific radiative emission processes. Specifically, the faster lifetime is dominated by emission from the main IR active mode  $\nu_9 \approx 1751$   $\text{cm}^{-1}$  ( $A_9^{10} \approx 1807$ ) and the slower lifetime attributed to emission from weaker modes  $\nu_{1,2} \approx 127\text{--}141$   $\text{cm}^{-1}$  ( $A_{1,2}^{10} \approx 21\text{--}30$ ). This double lifetime cooling is not apparent for  $C_3^-$  and  $C_4^-$  because the majority of the IR radiative cooling from the high frequency mode with a large  $A^{10}$  coefficient occurs on a subsecond time scale. The power emitted by each IR-active mode over the course of the SHC simulation (IVR included) for  $C_3^-$  (upper panel) and  $C_5^-$  (lower panel) is shown in Fig. 8. Comparing the two panels shows that the main IR active mode for  $C_5^-$  ( $\nu_9$ ) continues to contribute to cooling on the seconds time scale, while the analogous mode of  $C_3^-$  ( $\nu_4$ ) is no longer active. We expect that increasing molecular size, i.e.,  $n$  in the  $C_n^-$  series, will lead to increased IR cooling time scales in the ultraslow cooling regime.

#### IV. SUMMARY AND OUTLOOK

The present work has investigated the ultraslow cooling characteristics of three astrochemically relevant anions under conditions approximating a cold dark molecular cloud. Interestingly, an increase in the molecular size leads to longer average ion cooling lifetimes in the ultraslow cooling regime:  $3.1 \pm 0.1$  s for  $C_3^-$ ,  $6.8 \pm 0.5$  s for  $C_4^-$ , and  $24 \pm 5$  s for  $C_5^-$ . Variation in ion cooling lifetimes across the hot band is attributed to a distribution of internal energies. These are the first known measurements on carbonaceous anions extending to the ultraslow (seconds) time scale; all previous measurements have been performed under room temperature conditions and were restricted to measuring the subsecond cooling dynamics.

The increase in the average ion cooling lifetime with the molecular size can be understood by considering the point group symmetry ( $D_{\infty h}$ ) of the anions and that E1 radiative transitions require a change in electric dipole moment. In particular, the high symmetry means that each of the present anions have only three vibrational modes with  $A^{10}$  coefficients larger than 10. Although  $A^{10}$  coefficients for  $\sigma_u$ -symmetric vibrational modes quickly increase with the molecular size beyond  $C_5^-$ , for  $n = 3\text{--}5$ , there are an increasing number of low frequency modes with increasing  $n$  (mostly IR inactive) and the weakly IR active  $\pi_u$ -symmetric vibrational modes become lower in frequency and have lower radiative emission rates [see Eq. (2) and the supplementary material]. The net result is an increase in ion cooling lifetime with increasing  $n$  in the  $C_n^-$  series. These ion

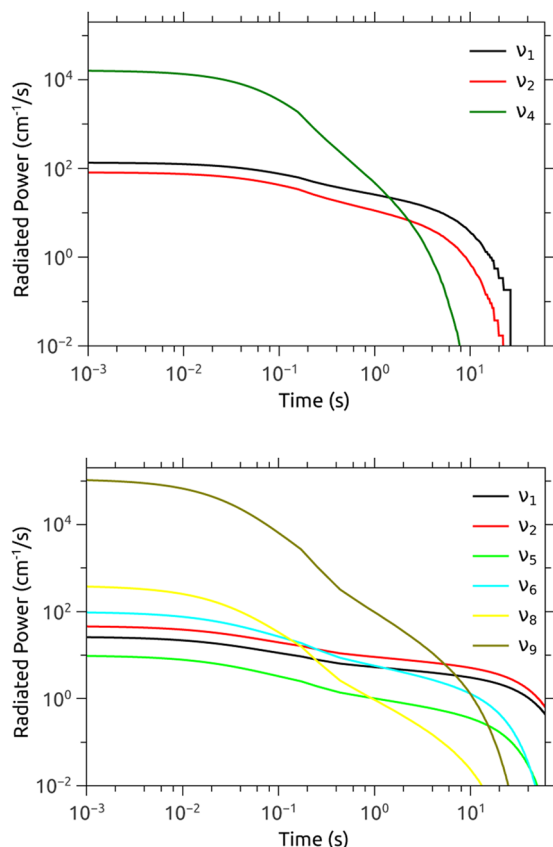


**FIG. 8.** Mode-specific radiated power for  $C_3^-$  (upper panel) and  $C_5^-$  (lower panel). Note the log-log scale in both panels. Mode  $\nu_4$  for  $C_3^-$  and mode  $\nu_9$  for  $C_5^-$  have  $\sigma_u$  symmetry.

cooling dynamics would not be evident at room temperature for  $n > 3$  because the average thermal vibrational energy exceeds the energy of the low frequency modes:  $\approx 342 \text{ cm}^{-1}$  ( $C_4^-$ ) and  $\approx 587 \text{ cm}^{-1}$  ( $C_5^-$ ) at 298 K assuming harmonic vibrational partition functions. We are presently applying the methods described in this work to study the ultraslow cooling dynamics of larger carbonaceous anions.

As part of the present study, we developed a simple harmonic cascade model that proved capable of simulating IR radiative emission using input data from conventional electronic structure calculations. With provision for IVR, the model qualitatively reproduced the experimental ion cooling lifetimes and provided a mode-by-mode understanding of the cooling dynamics. The agreement between theory and experiment provides confidence for applying this model to anions for which experimental data are not available or difficult to measure.

It is worth noting that the photodetachment spectra showed no clear vibrational structure, presumably due to the low resolution of the OPO laser and large wavelength increments—our measurements sacrificed spectral resolution for range and throughput to compare three anions in a series. Future studies might apply higher resolution light sources (e.g., dye lasers) to resolve resonant detaching transitions, hot-band structure, and to enable characterization of mode-specific ultraslow cooling properties. Furthermore, it should be noted that the application of the present 2D photodetachment methodology to larger molecular anions may prove more complicated due to near-threshold resonant excitations. Specifically, if there are substantial cross sections for photoexcitation of  $\pi\pi^*$  states situated below the detachment threshold or for resonances situated in the detachment continuum, ensuing autodetachment and internal conversion dynamics might affect the observed ion cooling lifetimes and spectral features. For example, experiments have shown that photoexcitation followed by internal conversion to recover the ground electronic state is efficient for  $C_n^-$  ( $n > 4$ ) and polycyclic aromatic hydrocarbon (PAH) anions,<sup>20,54–56</sup> with photoexcitation cross sections for optically allowed transitions in PAH anions generally being much larger than cross sections for direct photodetachment. If neutral formation through thermionic emission or dissociation processes takes longer than the time ions spend in the straight section of the ion storage ring after irradiation ( $\approx 4\text{--}5 \mu\text{s}$ ), then the neutrals formed outside of the straight section of the ion storage ring will not be counted by the “imaging detector.” Fortunately, in DESIREE, the relative importance of delayed neutral formation can be ascertained by simultaneously measuring neutral yield on the detector on the opposite straight section of the ion storage ring (glass plate/MCP detector in Fig. 1).

## SUPPLEMENTARY MATERIAL

See [supplementary material](#) for additional data on beam storage and radiative cooling lifetimes, Wigner threshold law fits, and details of our SHC models.

## ACKNOWLEDGMENTS

This work was supported by the Swedish Research Council (Grant Nos. 2015-04990, 2016-03675, 2016-04181, and 2018-04092) and the Swedish Foundation for International Collaboration in

Research and Higher Education (STINT, Grant No. PT2017-7328 awarded to J.N.B., E.C., and M.H.S.). We acknowledge the DESIREE infrastructure for provisioning of facilities and experimental support, and thank the operators and technical staff for their invaluable assistance. The DESIREE infrastructure receives funding from the Swedish Research Council under Grant No. 2017-00621.

## REFERENCES

- 1 M. Larsson, W. D. Geppert, and G. Nyman, *Rep. Prog. Phys.* **75**, 066901 (2012).
- 2 T. J. Millar, C. Walsh, and T. A. Field, *Chem. Rev.* **117**, 1765 (2017).
- 3 M. C. McCarthy, C. A. Gottlieb, H. Gupta, and P. Thaddeus, *Astrophys. J.* **652**, L141 (2006).
- 4 J. Cernicharo, M. Guélin, M. Agúndez, K. Kawaguchi, M. McCarthy, and P. Thaddeus, *Astron. Astrophys.* **467**, L37 (2007).
- 5 S. Brünken, H. Gupta, C. A. Gottlieb, M. C. McCarthy, and P. Thaddeus, *Astrophys. J.* **664**, L43 (2007).
- 6 M. Agúndez, J. Cernicharo, M. Guélin, C. Kahane, E. Roueff, J. Klos, F. J. Aoi, F. Lique, N. Marcelino, J. R. Goicoechea, M. G. García, C. A. Gottlieb, M. C. McCarthy, and P. Thaddeus, *Astron. Astrophys.* **517**, L2 (2010).
- 7 P. Thaddeus, C. A. Gottlieb, H. Gupta, S. Brunken, and M. C. McCarthy, *Astrophys. J.* **677**, L132 (2008).
- 8 J. Cernicharo, M. Guélin, M. Agúndez, M. C. McCarthy, and P. Thaddeus, *Astrophys. J.* **688**, L83 (2008).
- 9 E. Herbst, *Phys. Chem. Chem. Phys.* **16**, 3344 (2014).
- 10 F. Carelli, M. Satta, T. Grassi, and F. A. Gianturco, *Astrophys. J.* **774**, 97 (2013).
- 11 E. Roueff and F. Lique, *Chem. Rev.* **113**, 8906 (2013).
- 12 E. Roueff and E. Herbst, *J. Phys.: Conf. Ser.* **192**, 012008 (2009).
- 13 D. Gerlich and M. Smith, *Phys. Scr.* **73**, C25 (2006).
- 14 K. W. Hinkle, J. J. Keady, and P. F. Bernath, *Science* **241**, 1319 (1988).
- 15 P. F. Bernath, K. H. Hinkle, and J. J. Keady, *Science* **244**, 562 (1989).
- 16 M. Khamesian, N. Douguet, S. F. dos Santos, O. Dulieu, M. Raoult, W. J. Briggs, and V. Kokoouline, *Phys. Rev. Lett.* **117**, 123001 (2016).
- 17 N. Sakai, T. Sakai, Y. Osamura, and S. Yamamoto, *Astrophys. J.* **667**, L65 (2007).
- 18 E. A. Bergin and M. Tafalla, *Annu. Rev. Astron. Astrophys.* **45**, 339 (2007).
- 19 H. T. Schmidt, G. Eklund, K. C. Chartkunchand, E. K. Anderson, M. Kamińska, N. de Ruelle, R. D. Thomas, M. K. Kristiansson, M. Gatchell, P. Reinherd *et al.*, *Phys. Rev. Lett.* **119**, 073001 (2017).
- 20 Y. Zhao, E. de Beer, C. Xu, T. Taylor, and D. M. Neumark, *J. Chem. Phys.* **105**, 4905 (1996).
- 21 A. Léger, P. Boissel, and L. d’Hendecourt, *Phys. Rev. Lett.* **60**, 921 (1988).
- 22 G. Ito, T. Furukawa, H. Tanuma, J. Matsumoto, H. Shiromaru, T. Majima, M. Goto, T. Azuma, and K. Hansen, *Phys. Rev. Lett.* **112**, 183001 (2014).
- 23 N. Kono, T. Furukawa, H. Tanuma, J. Matsumoto, H. Shiromaru, T. Azuma, K. Najafian, M. S. Pettersson, B. Dynefors, and K. Hansen, *Phys. Chem. Chem. Phys.* **17**, 24732 (2015).
- 24 Y. Ebara, T. Furukawa, J. Matsumoto, H. Tanuma, T. Azuma, H. Shiromaru, and K. Hansen, *Phys. Rev. Lett.* **117**, 133004 (2016).
- 25 N. Kono, R. Suzuki, T. Furukawa, J. Matsumoto, H. Tanuma, H. Shiromaru, T. Azuma, and K. Hansen, *Phys. Rev. A* **98**, 063434 (2018).
- 26 H. Shiromaru, T. Furukawa, G. Ito, N. Kono, H. Tanuma, J. Matsumoto, M. Goto, T. Majima, A. E. K. Sundén, K. Najafian, M. S. Pettersson, B. Dynefors, K. Hansen, and T. Azuma, *J. Phys.: Conf. Ser.* **635**, 012035 (2015).
- 27 C. Meyer, A. Becker, K. Blaum, C. Breitenfeldt, S. George, J. Göck, M. Grieser, F. Grussie, E. A. Guerin, R. von Hahn, P. Herwig, C. Krantz, H. Kreckel, J. Lion, S. Lohmann, P. M. Mishra, O. Novotný, A. P. O’Connor, R. Repnow, S. Saurabh, D. Schwalm, L. Schweikhard, K. Spruck, S. Sunil Kumar, S. Vogel, and A. Wolf, *Phys. Rev. Lett.* **119**, 023202 (2017).
- 28 R. von Hahn, A. Becker, F. Berg, K. Blaum, C. Breitenfeldt, H. Fadil, F. Fellenberger, M. Froese, S. George, J. Göck, M. Grieser, F. Grussie, E. A. Guerin, O. Heber, P. Herwig, J. Kartheim, C. Krantz, H. Kreckel, M. Lange, F. Laux, S. Lohmann, S. Menk, C. Meyer, P. M. Mishra, O. Novotný, A. P. O’Connor, D. A. Orlov, M. L. Rappaport, R. Repnow, S. Saurabh, S. Schippers, C. D. Schröter,

- D. Schwalm, L. Schweikhard, T. Sieber, A. Shornikov, K. Spruck, S. Sunil Kumar, J. Ullrich, X. Urbain, S. Vogel, P. Wilhelm, A. Wolf, and D. Zajfman, *Rev. Sci. Instrum.* **87**, 063115 (2016).
- <sup>29</sup>Y. Nakano, Y. Enomoto, T. Masunaga, S. Menk, P. Bertier, and T. Azuma, *Rev. Sci. Instrum.* **88**, 033110 (2017).
- <sup>30</sup>K. C. Chartkunchand, M. Kamińska, E. K. Anderson, M. K. Kristiansson, G. Eklund, O. M. Hole, R. F. Nascimento, M. Blom, M. Björkhage, A. Källberg, P. Löfgren, P. Reinhed, S. Rosén, A. Simonsson, R. D. Thomas, S. Mannervik, V. T. Davis, P. A. Neill, J. S. Thompson, D. Hanstorp, H. Zettergren, H. Cederquist, and H. T. Schmidt, *Phys. Rev. A* **94**, 032501 (2016).
- <sup>31</sup>A. P. O'Connor, A. Becker, K. Blaum, C. Breitenfeldt, S. George, J. Göck, M. Grieser, F. Grussie, E. A. Guerin, R. von Hahn, U. Hechtischer, P. Herwig, J. Kartheim, C. Krantz, H. Kreckel, S. Lohmann, C. Meyer, P. M. Mishra, O. Novotný, R. Repnow, S. Saurabh, D. Schwalm, K. Spruck, S. Sunil Kumar, S. Vogel, and A. Wolf, *Phys. Rev. Lett.* **116**, 113002 (2016).
- <sup>32</sup>K. Hansen, M. H. Stockett, M. Kamińska, R. F. Nascimento, E. K. Anderson, M. Gatchell, K. C. Chartkunchand, G. Eklund, H. Zettergren, H. T. Schmidt, and H. Cederquist, *Phys. Rev. A* **95**, 022511 (2017).
- <sup>33</sup>E. K. Anderson, M. Kamińska, K. C. Chartkunchand, G. Eklund, M. Gatchell, K. Hansen, H. Zettergren, H. Cederquist, and H. T. Schmidt, *Phys. Rev. A* **98**, 022705 (2018).
- <sup>34</sup>A. Naaman, K. G. Bhushan, H. B. Pedersen, N. Altstein, O. Heber, M. L. Rappaport, R. Moalem, and D. Zajfman, *J. Chem. Phys.* **113**, 4662 (2000).
- <sup>35</sup>M. Goto, A. Sundén, H. Shiromaru, J. Matsumoto, H. Tanuma, T. Azuma, and K. Hansen, *J. Chem. Phys.* **139**, 054306 (2013).
- <sup>36</sup>V. Chandrasekaran, B. Kafle, A. Prabhakaran, O. Heber, M. Rappaport, H. Rubinstein, D. Schwalm, Y. Toker, and D. Zajfman, *J. Phys. Chem. Lett.* **5**, 4078 (2014).
- <sup>37</sup>K. Saha, A. Prabhakaran, V. Chandrasekaran, M. L. Rappaport, O. Heber, and D. Zajfman, *Rev. Sci. Instrum.* **88**, 053101 (2017).
- <sup>38</sup>R. D. Thomas, H. T. Schmidt, G. Andler, M. Björkhage, M. Blom, L. Brännholm, E. Bäckström, H. Danared, S. Das, N. Haag, P. Halldén, F. Hellberg, A. I. S. Holm, H. A. B. Johansson, A. Källberg, G. Källersjö, M. Larsson, S. Leontein, L. Liljeby, P. Löfgren, B. Malm, S. Mannervik, M. Masuda, D. Misra, A. Orbán, A. Paál, P. Reinhed, K.-G. Rensfelt, S. Rosén, K. Schmidt, F. Seitz, A. Simonsson, J. Weimer, H. Zettergren, and H. Cederquist, *Rev. Sci. Instrum.* **82**, 065112 (2011).
- <sup>39</sup>H. T. Schmidt, R. D. Thomas, M. Gatchell, S. Rosén, P. Reinhed, P. Löfgren, L. Brännholm, M. Blom, M. Björkhage, E. Bäckström, J. D. Alexander, S. Leontein, D. Hanstorp, H. Zettergren, L. Liljeby, A. Källberg, A. Simonsson, F. Hellberg, S. Mannervik, M. Larsson, W. D. Geppert, K. G. Rensfelt, H. Danared, A. Paál, M. Masuda, P. Halldén, G. Andler, M. H. Stockett, T. Chen, G. Källersjö, J. Weimer, K. Hansen, H. Hartman, and H. Cederquist, *Rev. Sci. Instrum.* **84**, 055115 (2013).
- <sup>40</sup>E. Bäckström, D. Hanstorp, O. M. Hole, M. Kamińska, R. F. Nascimento, M. Blom, M. Björkhage, A. Källberg, P. Löfgren, P. Reinhed, S. Rosén, A. Simonsson, R. D. Thomas, S. Mannervik, H. T. Schmidt, and H. Cederquist, *Phys. Rev. Lett.* **114**, 143003 (2015).
- <sup>41</sup>S. Rosén, H. T. Schmidt, P. Reinhed, D. Fischer, R. D. Thomas, H. Cederquist, L. Liljeby, L. Bagge, S. Leontein, and M. Blom, *Rev. Sci. Instrum.* **78**, 113301 (2007).
- <sup>42</sup>I. T. Jolliffe, *Principal Component Analysis*, Springer Series in Statistics, 2nd ed. (Springer, 2002).
- <sup>43</sup>M. H. Stockett, M. Björkhage, H. Cederquist, H. Schmidt, and H. Zettergren, *Faraday Discuss.* **217**, 126 (2019).
- <sup>44</sup>E. P. Wigner, *Phys. Rev.* **73**, 1002 (1948).
- <sup>45</sup>J. W. Farley, *Phys. Rev. A* **40**, 6286 (1989).
- <sup>46</sup>J.-D. Chai and M. Head-Gordon, *Phys. Chem. Chem. Phys.* **10**, 6615 (2008).
- <sup>47</sup>T. H. Dunning, Jr., *J. Chem. Phys.* **90**, 1007 (1989).
- <sup>48</sup>Y. Shao, Z. Gan, E. Epifanovsky, A. T. Gilbert, M. Wormit, J. Kussmann, A. W. Lange, A. Behn, J. Deng, X. Feng, D. Ghosh, M. Goldey, P. R. Horn, L. D. Jacobson, I. Kaliman, R. Z. Khaliullin, T. Kus, A. Landau, J. Liu, E. I. Proynov, Y. M. Rhee, R. M. Richard, M. A. Rohrdanz, R. P. Steele, E. J. Sundstrom, H. L. Woodcock III, P. M. Zimmerman, D. Zuev, B. Albrecht, E. Alguire, B. Austin, G. J. O. Beran, Y. A. Bernard, E. Berquist, K. Brandhorst, K. B. Bravaya, S. T. Brown, D. Casanova, C.-M. Chang, Y. Chen, S. H. Chien, K. D. Closser, D. L. Crittenden, M. Diedenhofen, R. A. DiStasio, Jr., H. Do, A. D. Dutoi, R. G. Edgar, S. Fatehi, L. Fusti-Molnar, A. Ghysels, A. Golubeva-Zadorozhnaya, J. Gomes, M. W. Hanson-Heine, P. H. Harbach, A. W. Hauser, E. G. Hohenstein, Z. C. Holden, T.-C. Jagau, H. Ji, B. Kaduk, K. Khistyayev, J. Kim, J. Kim, R. A. King, P. Klunzinger, D. Kosenkov, T. Kowalczyk, C. M. Krauter, K. U. Lao, A. D. Laurent, K. V. Lawler, S. V. Levchenko, C. Y. Lin, F. Liu, E. Livshits, R. C. Lochan, A. Luenser, P. Manohar, S. F. Manzer, S.-P. Mao, N. Mardirossian, A. V. Marenich, S. A. Maurer, N. J. Mayhall, E. Neuscamman, C. M. Oana, R. Olivares-Amaya, D. P. O'Neill, J. A. Parkhill, T. M. Perrine, R. Peverati, A. Prociuk, D. R. Rehn, E. Rosta, N. J. Russ, S. M. Sharada, S. Sharma, D. W. Small, A. Sodt, T. Stein, D. Stück, Y.-C. Su, A. J. Thom, T. Tsuchimoto, V. Vanovschi, L. Vogt, O. Vydrov, T. Wang, M. A. Watson, J. Wenzel, A. White, C. F. Williams, J. Yang, S. Yeganeh, S. R. Yost, Z.-Q. You, I. Y. Zhang, X. Zhang, Y. Zhao, B. R. Brooks, G. K. Chan, D. M. Chipman, C. J. Cramer, W. A. Goddard III, M. S. Gordon, W. J. Hehre, A. Klamt, H. F. Schaefer III, M. W. Schmidt, C. D. Sherrill, D. G. Truhlar, A. Warshel, X. Xu, A. Aspuru-Guzik, R. Baer, A. T. Bell, N. A. Besley, J.-D. Chai, A. Dreuw, B. D. Dunietz, T. R. Furlani, S. R. Gwaltney, C.-P. Hsu, Y. Jung, J. Kong, D. S. Lambrecht, W. Liang, C. Ochsenfeld, V. A. Rassolov, L. V. Slipchenko, J. E. Subotnik, T. V. Voorhis, J. M. Herbert, A. I. Krylov, P. M. W. Gill, and M. Head-Gordon, *Mol. Phys.* **113**, 184 (2015).
- <sup>49</sup>D. J. Nesbitt and R. W. Field, *J. Phys. Chem.* **100**, 12735 (1996).
- <sup>50</sup>J. Szczepanski, S. Ekern, and M. Vala, *J. Phys. Chem. A* **101**, 1841 (1997).
- <sup>51</sup>D. W. Arnold, S. E. Bradforth, T. N. Kitsopoulos, and D. M. Neumark, *J. Phys. Chem.* **95**, 8753 (1991).
- <sup>52</sup>T. N. Kitsopoulos, C. J. Chick, Y. Zhao, and D. M. Neumark, *J. Chem. Phys.* **95**, 5479 (1991).
- <sup>53</sup>C. Hock, J. B. Kim, M. L. Weichman, T. I. Yacovitch, and D. M. Neumark, *J. Chem. Phys.* **137**, 244201 (2012).
- <sup>54</sup>B. Baguenard, J. C. Pinaré, F. Lépine, C. Bordas, and M. Broyer, *Chem. Phys. Lett.* **352**, 147 (2002).
- <sup>55</sup>J. N. Bull, C. W. West, and J. R. R. Verlet, *Chem. Sci.* **6**, 1578 (2015).
- <sup>56</sup>J. N. Bull, C. W. West, and J. R. R. Verlet, *Phys. Chem. Chem. Phys.* **17**, 32464 (2015).